THE JOURNAL OF PHYSICAL CHEMISTRY C

Article

pubs.acs.org/JPCC

Coincidence Lattices of 2D Crystals: Heterostructure Predictions and Applications

Daniel S. Koda,*,† Friedhelm Bechstedt,*,‡ Marcelo Marques,*,† and Lara K. Teles*,†

†Grupo de Materiais Semicondutores e Nanotecnologia, Instituto Tecnológico de Aeronáutica, DCTA, 12228-900 São José dos Campos, Brazil

‡Institut für Festkörpertheorie und -optik, Friedrich-Schiller-Universität, Max-Wien-Platz 1, D-07743 Jena, Germany

Supporting Information

ABSTRACT: van der Waals heterostructures provide many novel applications due to a combination of properties. However, their experimental construction and theoretical simulation suffer from the incommensurability of 2D crystals with respect to their symmetry and their lattice constants. In this work, we present a simplified method to predict favorable combinations of 2D crystals based on the coincidence lattice method. We present a huge set of possible heterostructures made from transition-metal dichalcogenides, group IV dichalcogenides, graphene, and hexagonal boron nitride. The method is then validated for theoretically and experimentally studied 2D crystals and van der Waals-bonded heterostructures. The power of the approach is demonstrated by comparison of resulting supercell sizes, strain, and relative orientation with experimental and theoretical data available. To display the prospects of this approach, we simulate three heterostructures and analyze the resulting structural and electronic properties, finding favorable stackings and small changes in band alignments in the weakly interacting heterojunction.

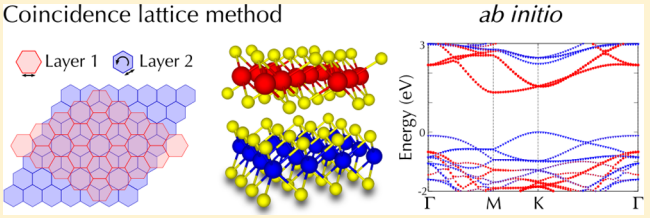

I. INTRODUCTION

Two-dimensional (2D) crystals such as graphene (Gr), hexagonal boron nitride (hBN), transition-metal dichalcogenides (TMDCs), phosphorene, and many others[1] have paved the way to novel physics and device applications. Their unique electronic, optical and mechanical properties show great promise for their combination in atomically thin flexible devices based solely on 2D layers.[2,3] Combinations of such different 2D crystals in van der Waals (vdW) heterostructures further expand the range of tunable properties and new devices.[4] The appearance of an interface between two different sheet crystals broadens the variation of possible properties by diverse stackings. This is important when comparing with the properties of isolated atomic layers, offering additional ease of tuning by doping, alloying, straining, or applying external electric fields. Other fascinating modifications may be matches in vdW-bonded stacks leading to type I and type II heterostructures.[5] The alignment of the two electronic structures is controversially discussed in general, but it is specifically discussed for important TMDC/TMDC combinations, even among lattice-matched ones such as MoS_2 and WS_2.[6]

Despite the easy preparation of vdW heterostructures by means of exfoliated 2D layers from vdW-bonded three-dimensional layered crystals, the resizing of the two lattices and their relative orientation, stacking, and strain effects are capable of changing the electronic properties of 2D crystals.[7,8] These influences become more important when considering the epitaxial growth of one layer on the other one, e.g., the vdW epitaxy of TMDC monolayers on graphene, for which a preferential orientation among the layers has been found.[9] Therefore, structure-induced effects on the interface formation and the electronic structure alignment cannot be overlooked.

In general, 2D heterostructures can be fabricated with a mismatch of crystal structures, lattice constants, and chemical bonding. Transitions between incommensurate states to commensurate ones have been observed in vdW-bonded stackings,[10] but in the majority of experimental studies these aspects are omitted. Theoretical investigations suffer from the problem of, in general, the incommensurability of the two layered systems. During modeling, usually, small 2D supercells are assumed with a certain stacking, orientation and, in particular, some strain.[6,11] Larger supercells, therefore with a reduced influence of these effects, increase the numerical efforts of quantum mechanical calculations within the density functional theory (DFT).[12] Hence, a certain compromise between determination of favorable arrangements and cell size is required.

In order to obtain important information concerning favorable relative arrangements of two 2D crystals in a generic heterostructure, we apply the coincidence lattice method derived from surface studies[13] to predict new possibilities for the simulation of vdW heterostructures. This includes finding supercells that require little computational effort to simulate,

Received: February 12, 2016
Revised: April 20, 2016
Published: April 26, 2016

DOI: 10.1021/acs.jpcc.6b01496
J. Phys. Chem. C 2016, 120, 10895−10908

despite being incommensurable, and assessing combinations with specific rotation angles. Contrary to the approach in similar studies,[6,14] we present a method which leads to more favorable stackings when one allows for specific interlayer twists. This enables theoretical studies to explore deeper possibilities within vdW-bonded systems, effects due to interlayer twist, or Moiré patterns despite limited computational resources.[15] Heterostructures tailored to match experimental data can also benefit from the technique. Theoretical structures can be easily created to emulate real-world samples.

The methodology for finding coincidence lattices is explained in section II, in which also successful examples of the developed approach are presented. Results are given and discussed in section III for a variety of the most interesting TMDCs, group IV dichalcogenides, graphene, and group III–V compounds. The application of this technique is also explored in the same section, in which three different bilayer systems built from favorable coincidences are simulated by adding the atoms, optimizing the atomic geometries, and calculating the electronic structures. Most of the results using the coincidence lattice method are summarized in Table S1 of the Supporting Information.

II. METHODOLOGY

Coincidence Lattice Method. We assume that the atomic geometries, i.e., the 2D Bravais lattices and the atomic basis, of the 2D crystals forming a bilayer heterostructure are known. Furthermore, we assume that the two layered systems are arranged in energetically favorable atomic positions despite their crystal structure, lattice constant, and bonding mismatches. In a first step, ab initio calculations of the total energy should not be performed to determine the relative positions of the two crystal lattices. Rather, we start from two isolated 2D Bravais lattices with given lattice constants (from ab initio calculations or measurements) and follow the idea to construct a coincidence lattice with a larger unit cell.[13] The physical principle of this idea is the realization of a joint lattice that leaves the energy of the bilayer system smaller by enhanced bonding at the interface when compared to the general orientations and translations of the two isolated crystals.

We denote the primitive basis vectors of the Bravais lattices of the 2D crystals a and b by

$$\begin{aligned}\mathbf{R}_a &= m_1\mathbf{a}_1 + m_2\mathbf{a}_2\\ \mathbf{R}_b &= n_1\mathbf{b}_1 + n_2\mathbf{b}_2\end{aligned} \tag{1}$$

in which m_i, $n_i \in \mathbb{Z}$, $i = 1, 2$ and $\mathbf{a}_i$ and $\mathbf{b}_i$ are the primitive vectors for each of the lattices. They are characterized by one or two lattice constants of the 2D crystal and the type of 2D Bravais lattice.[16] Linear combinations of these vectors with integer coefficients yield all lattice points of the corresponding 2D Bravais lattice. The relationship between these vectors and the unit cell area is given by

$$\begin{aligned}S_a &= |\mathbf{a}_1 \times \mathbf{a}_2|\\ S_b &= |\mathbf{b}_1 \times \mathbf{b}_2|\end{aligned} \tag{2}$$

The primitive basis vectors $\tilde{\mathbf{a}}_i$ and $\tilde{\mathbf{b}}_i$ of the coincidence lattice can be constructed by arbitrary linear mappings, denoted by the 2×2 matrices $\mathbf{M}^a$ and $\mathbf{M}^b$, taking into account all possible scalings and rotations

$$\begin{aligned}\begin{bmatrix}\tilde{\mathbf{a}}_1^{\mathrm{T}}\\ \tilde{\mathbf{a}}_2^{\mathrm{T}}\end{bmatrix} &= \mathbf{M}^a\begin{bmatrix}\mathbf{a}_1^{\mathrm{T}}\\ \mathbf{a}_2^{\mathrm{T}}\end{bmatrix}\\ \begin{bmatrix}\tilde{\mathbf{b}}_1^{\mathrm{T}}\\ \tilde{\mathbf{b}}_2^{\mathrm{T}}\end{bmatrix} &= \mathbf{M}^b\begin{bmatrix}\mathbf{b}_1^{\mathrm{T}}\\ \mathbf{b}_2^{\mathrm{T}}\end{bmatrix}\end{aligned} \tag{3}$$

where $\mathbf{a}_i^{\mathrm{T}}$,$\mathbf{b}_i^{\mathrm{T}}$ are line vectors, i.e. the transposed vectors of $\mathbf{a}_i$,$\mathbf{b}_i$.

In contrast to surface physics,[17] we restrict ourselves here to the case in which all elements from these transformation matrices are integer numbers in order to obtain sublattices of the original 2D Bravais lattices. Therefore, the areas of the corresponding unit cells are

$$\begin{aligned}|\tilde{\mathbf{a}}_1 \times \tilde{\mathbf{a}}_2| &= \det \mathbf{M}^a|\mathbf{a}_1 \times \mathbf{a}_2|\\ |\tilde{\mathbf{b}}_1 \times \tilde{\mathbf{b}}_2| &= \det \mathbf{M}^b|\mathbf{b}_1 \times \mathbf{b}_2|\end{aligned} \tag{4}$$

In surface physics[17] one speaks about a superstructure or a reconstruction of the original surface layers, characterized by a $\mathbf{M}$ matrix. Instead of the matrix notation introduced in eq 3, in most cases it is more convenient to use the so-called Wood notation,[18] which relates the supercell vectors $\{\tilde{\mathbf{a}}_i,\tilde{\mathbf{b}}_i\}$ to the original ones $\{\mathbf{a}_i,\mathbf{b}_i\}$ by means of a scaling and rotation denoted as

$$\begin{aligned}\left(\frac{|\tilde{\mathbf{a}}_1|}{|\mathbf{a}_1|} \times \frac{|\tilde{\mathbf{a}}_2|}{|\mathbf{a}_2|}\right)\mathrm{R}\phi_a\\ \left(\frac{|\tilde{\mathbf{b}}_1|}{|\mathbf{b}_1|} \times \frac{|\tilde{\mathbf{b}}_2|}{|\mathbf{b}_2|}\right)\mathrm{R}\phi_b\end{aligned} \tag{5}$$

with

$$\begin{aligned}\phi_a &= \arccos\left(\frac{\tilde{\mathbf{a}}_1\cdot\mathbf{a}_1}{|\tilde{\mathbf{a}}_1||\mathbf{a}_1|}\right)\\ \phi_b &= \arccos\left(\frac{\tilde{\mathbf{b}}_1\cdot\mathbf{b}_1}{|\tilde{\mathbf{b}}_1||\mathbf{b}_1|}\right)\end{aligned} \tag{6}$$

Rotations and displacements of original Bravais lattices, therefore, may generate sublattices, which may be equal in the commensurate case or almost equal in the incommensurate case. The latter situation may be transformed into a commensurate case by considering the two 2D crystals as slightly strained. In the commensurate limit, a coincidence lattice is defined by the same primitive basis vectors on both sides of the heterointerface

$$\begin{aligned}\tilde{\mathbf{a}}_1 &= \tilde{\mathbf{b}}_1\\ \tilde{\mathbf{a}}_2 &= \tilde{\mathbf{b}}_2\end{aligned} \tag{7}$$

which gives identical supercells on both sides with the same area

$$|\tilde{\mathbf{a}}_1 \times \tilde{\mathbf{a}}_2| = |\tilde{\mathbf{b}}_1 \times \tilde{\mathbf{b}}_2| \tag{8}$$

Such a supercell contains one coincidence lattice site.

To determine this supercell, we have to find two matrices $\mathbf{M}^a$ and $\mathbf{M}^b$ that fulfill the conditions of eq 7 and consequently of eq 8 as

DOI: 10.1021/acs.jpcc.6b01496
J. Phys. Chem. C 2016, 120, 10895−10908

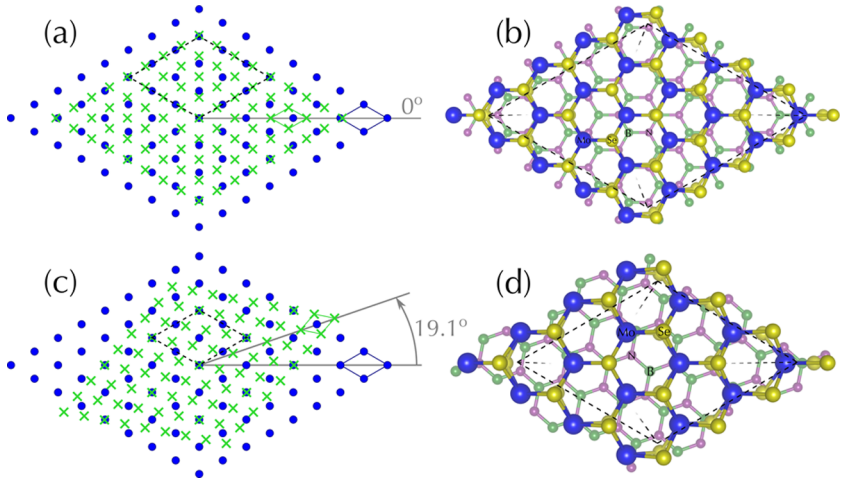

Figure 1. Matching of the hBN Bravais lattice (green crosses) and the $MoSe_2$ lattice (blue circles) (a) without rotation and (c) rotating both lattices by 19.1° against each other. The original unit cells are drawn with solid lines while the resulting supercell is shown with dashed lines. Atomic representations (perspective view) of the coincidence lattice method for $MoSe_2$ on top of hBN (b) without any rotation and (d) laterally rotated are also given. Molybdenum atoms are portrayed in blue, selenium atoms in yellow, boron atoms in green, and nitrogen in purple.

$$\mathbf{M}^{a}\begin{bmatrix}\mathbf{a}_1^{T}\\ \mathbf{a}_2^{T}\end{bmatrix} = \mathbf{M}^{b}\begin{bmatrix}\mathbf{b}_1^{T}\\ \mathbf{b}_2^{T}\end{bmatrix} \tag{9}$$

The desired solution is the one which minimizes the area (eq 8) of the supercell. In the incommensurate case, one requires that the conditions (eqs7−9) approximately match, so that a small strain should be applied to one or both 2D materials to obtain a commensurate situation.

In principle, one would have infinite solutions for supercells but only use a single one that has a minimum area. Therefore, it is possible to determine the two matrices $\mathbf{M}^a$ and $\mathbf{M}^b$ and, consequently, the desired supercell for the lattices by solving eqs 3, 8, and 9.

In a practical approach, it is sufficient to solve this problem as a system of diophantine equations through considerations that simplify the problem for computational solutions. To derive that simpler form, let $\theta = \phi_b - \phi_a$ be the relative rotation angle between these two lattices. As we have a degree of freedom for the angle of these planar lattices due the invariance of the conjoint Bravais arrangements to rotation, i.e., a simultaneous rotation of both lattices would not interfere with the relative distances of each point of the Bravais lattice with respect to all others points in the lattice, it would be redundant to specify two angles, one for each original lattice. Then, we can write a rotation matrix $\mathbf{M}$ to perform a relative rotation for only one of the two 2D crystals as

$$\mathbf{M} = \begin{bmatrix}\cos\theta & \sin\theta\\ -\sin\theta & \cos\theta\end{bmatrix} \tag{10}$$

We have to fulfill the requirement described in eq 7, which is equivalent to solving eq 9. Since $\mathbf{M}^a$ and $\mathbf{M}^b$ take into account scaling and rotation, we could solve this equation in two steps: first by fixing a given angle θ (and therefore the matrix $\mathbf{M}$) and second by stating the equivalence between eq 9 and the coincidence $\mathbf{R}_a = \mathbf{M}\mathbf{R}_b$, recurring from the notation of eq 1. If this coincidence occurs for at least three noncollinear points, this assures the existence, given the angle θ, of a supercell for the heterostructure. That is equivalent to find two nonzero and linearly independent solutions (m_1, m_2, n_1, n_2), $(m_1', m_2', n_1', n_2') \in \mathbb{Z}^4$ to the equation $\mathbf{R}_a = \mathbf{M}\mathbf{R}_b$, which can be rewritten using a linear system notation, introduced here as

$$\underbrace{[\mathbf{a}_1\ \mathbf{a}_2]}_{\mathbf{A}}\underbrace{\begin{bmatrix}m_1\\ m_2\end{bmatrix}}_{\mathbf{m}} = \mathbf{M}\underbrace{[\mathbf{b}_1\ \mathbf{b}_2]}_{\mathbf{B}}\underbrace{\begin{bmatrix}n_1\\ n_2\end{bmatrix}}_{\mathbf{n}}$$

$$\mathbf{Am} = \mathbf{MBn} \tag{11}$$

The desired solution is often the one that minimizes the area of the supercell, i.e., the vectors $\mathbf{m}$ and $\mathbf{m}'$ for which the area $|(\mathbf{Am}) \times (\mathbf{Am}')|$ is a minimum. That is analogous to simply finding the minimum ratio $|\mathbf{m} \times \mathbf{m}'|$ between the area of the supercell and the area of the unit cell. In this case, $|\mathbf{m}|$ and $|\mathbf{n}|$ are related to the size of the supercell compared to the size of the unit cell of the first and second 2D crystal, respectively. Using multiples of the original unit cells (e.g., a 2×2 supercell) for each one of the layer crystals would be equivalent to multiply the original solution $\mathbf{m}$ by a valid integer number. Multiplying the solution (m_1, m_2, n_1, n_2) by any nonzero integer would also return a solution for the same problem. That means that rotation and displacement of original Bravais lattices are both taken into account, just like the case described in the more general approach. The use of coincidence lattices for the simulation corresponds to the application of nonprimitive unit cells in terms of the original Bravais lattice. It, therefore, does not affect the electronic properties of each individual 2D crystal. The band gap and density of states remain unchanged. Only the band structure is modified due to its folding onto a correspondingly smaller Brillouin zone. The interaction between the individual 2D crystals in a heterostructure may give rise to modifications of the electronic properties.

As fluctuations in computed lattice parameters deduced using ab initio calculations would almost always lead to an incommensurate case of matching, we define a tolerance related to the maximum strain we would like to apply to each of the materials, in order to turn it into a commensurate case. These solutions are given by $|\mathbf{Am} - \mathbf{MBn}| < \text{TOLERANCE}$. In this case, the strain could be distributed between the two materials for optimal simulations according to the sensitivity of each one to an applied strain. It is also useful to limit the investigation of the supercells using an integer cutoff N_{max} as a stopping

DOI: 10.1021/acs.jpcc.6b01496
J. Phys. Chem. C 2016, 120, 10895−10908

criterion and hence limit the size of the supercells. More importantly, the θ angle must be specified as a parameter in this approach to impose a supercell creation with these specifications.

The application of the described method is useful not only to study the changes in the electronic structure with the rotation angle by using the smallest supercell, but also in cases in which the rotation does not play a significant role. In this latter case, it may lead to higher optimizations when comparing to the supercell creation, which does not consider the possibilities of rotations.

Good examples for illustration of the method are heterostructures made by two hexagonal 2D crystals, characterized by lattice constants a_a and a_b, in which the resulting coincidence lattice should also be hexagonal with a lattice constant $|\mathbf{m}|a_a = |\mathbf{n}|a_b$. To better illustrate the method, let us design a supercell of the bilayer heterostructure of hBN and molybdenum diselenide ($MoSe_2$), as depicted in Figure 1. With this example, we demonstrate the existence of a supercell of these two 2D crystals which is smaller when considering a relative rotation of 19.1° in comparison with a vanishing rotation between the two lattices. The latter would imply a supercell containing 59 atoms if both 2D compounds are biaxially strained by an absolute value of 0.73% (compressive for hBN and tensile for $MoSe_2$). On the other hand, applying a rotation leads to a smaller supercell, containing only 26 atoms, created with a smaller necessary strain with an absolute value of 0.33% (also compressive for hBN and tensile for $MoSe_2$) in order to make the two 2D systems commensurate.

To this point, no considerations about total energy are made, only predictions for the resulting supercell and coincidence lattice. Therefore, for a more precise description of their energetics, the resulting heterostructures, such as the ones displayed in Figure 1b,d, should be investigated with respect to their actual energies and resulting electronic (band) structures by means of ab initio simulations based on total energy and electronic structure methods.

Ab Initio Simulations. Calculations regarding structural, ground-state, and electronic properties were performed in this work using DFT as implemented in the Vienna Ab-initio Simulation Package (VASP).[19,20] The wave functions and pseudopotentials are generated within the projector-augmented wave (PAW) method.[21,22] The description of exchange and correlation (XC) was conducted using the Perdew–Burke–Ernzerhof (PBE) functional within the generalized gradient approximation (GGA).[23] The van der Waals interaction was taken in account using the optB86b functional.[24] It seems to predict structural parameters more accurately when compared with its counterparts without incurring into imprecise results for binding energies.[24,25] The kinetic energy cutoff for the plane waves is restricted to 500 eV and integrations over the 2D Brillouin zone (BZ) are performed using a 11 × 11 × 1 Γ-centered Monkhorst–Pack k-point mesh[26] for 1 × 1 lateral unit cells. The repeated slab method is applied to simulate individual 2D crystals.[17] A vacuum of 15 Å thickness is employed to ensure no unphysical interaction in the stacking direction. All structural parameters were calculated first, finding the energy minimum with a stopping criterion of 10^{-6} eV for the energy convergence and then relaxing the atomic positions until the Hellmann–Feynman forces on atoms were smaller than 1 meV/Å. Heterostructure investigations were performed after fixing the parameters of the most stable structural geometry of each monolayer and applying necessary strains to make the systems commensurate.

Electronic properties calculated using the optB86b functional lead to 2D band structures which suffer from the typical underestimation of energy gaps and interband distances computed as differences of Kohn–Sham eigenvalues of the DFT.[27] We take approximately the quasiparticle gap corrections into account by applying a XC hybrid functional HSE06[27−30] to compute the electronic structures. It simulates the important spatial nonlocality of the quasiparticle self-energy in GW approximation.[31]

Visualizations of supercells and structures were done with the software VESTA.[32]

III. RESULTS AND DISCUSSION

Monolayer 2D materials. In order to construct coincidence lattices and obtain heterostructure properties of the 2D crystals on top of each other, we need a unique database for the isolated 2D materials of interest. Experimental lattice constants suffer from different preparation and measurement techniques.[24,25] Theoretical lattice constants are available for the majority of 2D materials of interest for this work,[25] which are essentially hexagonal lattices with one lattice constant. However, the coincidence lattice method asks for an unified data set. Thus, we have to repeat the calculations by considering the same numerical approach with respect to XC functional energy cutoff and k-point sampling. After finding the coincidence lattices, we need to refine the atomic geometries to discuss consequences on the energetics and electronic structures of the heterostructures. Exactly the same numerical approach as in the case of the isolated layers can be applied to the heterostructures.

Indeed, to obtain the structural parameters for the isolated sheet materials, we have employed the optB86b functional to minimize deviations from the experimental lattice parameters.[24,25] This allows reasonable predictions of heterostructures that are not influenced by fluctuations of measured values by different groups and can be fully relaxed using one and the same method. It is important to mention that the actual lattice parameters influence the electronic structure; for instance, smaller lattice constants could lead to larger quasiparticle band gaps and vice versa.[33]

Here, we focus mainly on heterostructures made by two hexagonal sheet crystals. Thereby, apart from the flat monolayers graphene and hBN, we investigate 2D crystals consisting of triple atomic layers such as TMDCs and group IV dichalcogenides. Results for combination of such hexagonal crystals with rectangular ones, e.g. phosphorene, are discussed later. The triple-layer systems occur in different polymorphs, mainly 1T and 2H, which represent respectively octahedral (CdI_2-like) or trigonal prismatic coordination.[34] Phase transitions between them, sometimes accompanied by a semiconductor–metal transition as in MoS_2, may happen.[35] We choose here the most stable phase of a TMDC according to Zhuang and Hennig.[34] In the case of the Sn dichalcogenides, we use the energetically favorable 1T phase.[36] We should remark, however, that as far as we know, WTe_2 and $TaTe_2$ have not been observed experimentally in the phase here investigated. This is due to the existence of a more stable configuration in a distorted 1T phase,[37,38] which also alters the electronic properties of these materials. Yet, in this work, this phase transition is not taken into consideration, leading to simulations and coincidence lattice predictions for the

DOI: 10.1021/acs.jpcc.6b01496
J. Phys. Chem. C 2016, 120, 10895−10908

Table 1. Structural and Electronic Properties of Selected Monolayer 2D Crystals[a]

	a (Å)	a_{exp} (Å)	d_{MX} (Å)	E_g (eV)	A (eV)	I (eV)
graphene	2.467	2.456	1.42	0	4.861	4.861
hBN	2.512	2.510	1.45	5.79	0.941	6.735
HfS_2 (1T)	3.626	3.635	2.55	2.03	4.925	6.956
$HfSe_2$ (1T)	3.734	3.748	2.67	1.18	4.829	6.008
$HfTe_2$ (1T)	3.920	3.957	2.88	semimetal	4.670	4.670
MoS_2 (2H)	3.164	3.162	2.41	2.25	4.025	6.270
$MoSe_2$ (2H)	3.301	3.289	2.54	1.95	3.735	5.685
$MoTe_2$ (2H)	3.528	3.518	2.73	1.57	3.558	5.123
NbS_2 (2H)	3.340	3.310	2.49	metal	6.202	6.202
$NbSe_2$ (2H)	3.641	3.442	2.62	metal	5.847	5.847
$NbTe_2$ (2H)	3.663	3.680	2.81	metal	5.150	5.150
PtS_2 (1T)	3.566	3.542	2.40	2.64	4.355	6.992
$PtSe_2$ (1T)	3.728	3.727	2.53	1.91	4.218	6.129
$PtTe_2$ (1T)	3.988	4.026	2.70	1.08	3.913	4.990
SnS_2 (1T)	3.667	3.648	2.59	2.36	4.955	7.315
$SnSe_2$ (1T)	3.831	3.811	2.73	1.38	5.112	6.493
TaS_2 (2H)	3.321	3.364	2.48	metal	6.024	6.024
$TaSe_2$ (2H)	3.449	3.476	2.63	metal	5.432	5.432
$TaTe_2$ (2H)	3.674	–	2.80	metal	5.026	5.026
TiS_2 (1T)	3.375	3.409	2.42	0.47	5.559	6.029
$TiSe_2$ (1T)	3.499	3.536	2.55	semimetal	5.213	5.213
$TiTe_2$ (1T)	3.705	3.777	2.76	metal	4.777	4.777
VS_2 (1T)	3.153	3.221	2.34	metal	5.482	5.482
VSe_2 (1T)	3.305	3.358	2.48	metal	5.256	5.256
WS_2 (2H)	3.182	3.153	2.43	2.29	3.782	6.073
WSe_2 (2H)	3.296	3.282	2.54	2.11	3.325	5.430
WTe_2 (2H)	3.527	–	2.73	1.52	3.395	4.918
ZrS_2 (1T)	3.650	3.662	2.57	1.85	5.138	6.989
$ZrSe_2$ (1T)	3.768	3.770	2.69	1.10	4.996	6.091
$ZrTe_2$ (1T)	3.926	3.952	2.90	semimetal	4.839	4.839

[a]The lattice parameter (a) and the bond length (d_{MX}) are calculated with the optB86b functional, whereas the band gap (E_g) is obtained from a subsequent HSE06 calculation. The ionization energy (I) and electron affinity (A) are referred to the vacuum level. Experimental lattice parameters (a_{exp}) are taken from the collection in refs 25, 40, 41. The most stable polymorph according to ref 34, 1T or 2H, is studied.

theoretical 2H conformation phase with hexagonal Bravais lattices.

Results for the relaxed, isolated 2D materials are presented in Table 1. The lattice parameters are in excellent agreement with the bulk experimental values, and the interchange between underestimation/overestimation has been predicted in a previous work.[25] For better structural characterization of the neutral triple atomic layers, in Table 1 we also list the bond length between a metal (M) atom in the central atomic layer and a neighboring chalcogen (X) atom in a layer above or below the central one. The expectation that the GGA-like XC functional optB86b gives slightly overestimated lattice constants is not only fulfilled for graphene and hBN but also for dichalcogenides with VIA, VIIA, and IVB elements from the periodic table. The dichalcogenides of transition-metal atoms from the groups IVA and VA, however, show the opposite behavior.

For studies beyond finding coincidence lattices, such as the influence of these superstructures on the electronic properties, e.g., band alignments in corresponding heterostructures, characteristic band structure parameters of the isolated 2D crystals are also given in Table 1. Quasiparticle effects are approximately simulated using the nonlocal exchange−correlation functional HSE06.[29,30] We use the HSE06 approach despite the seeming underestimation of the quasiparticle shifts[31] with respect to calculations in the framework of the GW approach.[39] For a given transition-metal atom there is a clear trend with the chalcogen atom. The fundamental gaps (in the case of a semiconducting phase) become smaller along the column S → Se → Te. The 3d, 4d, and 5d transition-metal cations have also a significant influence. In the case of group VB elements and for Ti, there is a clear tendency for a metallic behavior independent of the 1T or 2H polymorph. In addition to the fundamental gap, also the electron affinity A and the ionization potential I are listed. The description of the surface barriers of the 2D crystals with respect to the vacuum level has been determined as the plateau of the electrostatic potential between the material slabs.[17] Their values will be used later to determine natural band discontinuities between two 2D crystals via a vacuum-level alignment for the purpose of comparison.

All DFT calculations giving the results in Table 1 have been performed using primitive unit cells of the 2D crystals. Below, in the case of bilayer heterostructures with coincidence lattices, however, larger nonprimitive unit cells are investigated. As a consequence, also in the limit of vanishing interlayer interactions, smaller Brillouin zones are considered, resulting in folded band structures.

Prediction of Coincidence Lattices. Using the calculated lattice parameters in Table 1 for the investigated monolayer 2D materials and the procedure described in the section Coincidence Lattice Method, in Table S1 of the Supporting Information (SI) we predict the coincidence lattices of almost

DOI: 10.1021/acs.jpcc.6b01496
J. Phys. Chem. C 2016, 120, 10895−10908

Table 2. Coincidence Lattice Predictions of Supercells for Systems Studied in the Literature[6,7,42,46,47] [a]

heterobilayer	layer 1	layer 2	θ (deg)	N	ε (%)
		Experimental Bilayer Graphene Moiré Patterns (as in ref 42)			
Gr/Gr	$(\sqrt{300} \times \sqrt{300})$R30.0°	$(\sqrt{301} \times \sqrt{301})$R3.3°	3.3	1202	±0.08
Gr/Gr	$(\sqrt{91} \times \sqrt{91})$R27.0°	$(\sqrt{91} \times \sqrt{91})$R27.0°	6.0	364	±0.00
Gr/Gr	$(\sqrt{37} \times \sqrt{37})$R25.3°	$(\sqrt{37} \times \sqrt{37})$R25.3°	9.4	148	±0.00
		Theoretical Moiré Patterns of Graphene on top of hBN (as in ref 43)			
Gr/hBN	56 × 56	55 × 55	0.0	12322	±0.00
Gr/hBN	37 × 37	36 × 36	0.0	5330	∓0.47
		Experimental WSe_2/MoS_2 Heterobilayer (as in ref 46)			
WSe_2/MoS_2	$(\sqrt{19} \times \sqrt{19})$R23.4°	$(\sqrt{21} \times \sqrt{21})$R10.9°	12.5	120	±0.46
		Theoretical Graphene/MoS_2 Heterobilayers (as in ref 7)			
Gr/MoS_2	$(\sqrt{21} \times \sqrt{21})$R10.9°	$(\sqrt{13} \times \sqrt{13})$R13.9°	3.0	81	±0.45
Gr/MoS_2	$(\sqrt{43} \times \sqrt{43})$R7.6°	5 × 5	7.6	161	∓1.12
Gr/MoS_2	$(\sqrt{39} \times \sqrt{39})$R16.1°	5 × 5	16.1	153	±1.32
Gr/MoS_2	$(\sqrt{7} \times \sqrt{7})$R19.1°	2 × 2	19.1	26	∓1.55
Gr/MoS_2	$(\sqrt{21} \times \sqrt{21})$R10.9°	$(\sqrt{13} \times \sqrt{13})$R13.9°	24.8	81	±0.45
Gr/MoS_2	8 × 8	$(\sqrt{37} \times \sqrt{37})$R25.3°	25.3	239	∓1.26
		Experimental MoS_2 Bilayers (as in ref 47)			
MoS_2/MoS_2	$(\sqrt{13} \times \sqrt{13})$R13.9°	$(\sqrt{13} \times \sqrt{13})$R13.9°	27.8	78	±0.00
MoS_2/MoS_2	$(\sqrt{39} \times \sqrt{39})$R16.1°	$(\sqrt{43} \times \sqrt{43})$R7.6°	51.5	246	±2.44
		Theoretical Heterobilayers with MoS_2 (as in ref 6)			
MoS_2/WS_2	1 × 1	1 × 1	0.0	6	±0.28
MoS_2/hBN	$(\sqrt{13} \times \sqrt{13})$R13.9°	$(\sqrt{21} \times \sqrt{21})$R10.9°	3.0	81	±0.45
$MoS_2/MoTe_2$	4 × 4	$(\sqrt{13} \times \sqrt{13})$R13.9°	13.9	87	±0.25
$MoS_2/MoSe_2$	$(\sqrt{13} \times \sqrt{13})$R13.9°	$(\sqrt{12} \times \sqrt{12})$R30.0°	16.1	75	±0.12
MoS_2/Gr	4 × 4	$(\sqrt{27} \times \sqrt{27})$R30.0°	30.0	102	±0.64
		Our Predictions for Smaller Systems among the Ones from Ref 6			
MoS_2/Gr	$(\sqrt{13} \times \sqrt{13})$R13.9°	$(\sqrt{21} \times \sqrt{21})$R10.9°	3.0	81	∓0.45
MoS_2/hBN	$(\sqrt{12} \times \sqrt{12})$R30.0°	$(\sqrt{19} \times \sqrt{19})$R23.4°	6.6	74	∓0.05
$MoS_2/MoTe_2$	3 × 3	$(\sqrt{7} \times \sqrt{7})$R19.1°	19.1	48	∓0.84

[a]The column labeled as layer 1 or 2 relates the original monolayer unit cell in Wood notation[17,18] to the supercell used in the heterostructure, rotated by an angle θ with respect to each other. The first compound shown in the heterobilayer column is denoted as layer 1. The predicted number N of atoms inside the supercell and the equally distributed biaxial strain ε also characterize the building of the supercell. All lattice parameters used were the ones from this work's optimizations. The ± sign indicates a tensile strain used on layer 1 and a compression strain on layer 2, and vice versa for the ∓ sign.

strain-free 2D crystals in vdW-bonded heterostructures. Special care is taken for the supercell of the coincidence lattice, which is expressed by a superstructure of each of the two 2D crystals combined. Essentially, the results are presented using the Wood notation in the form shown in eq 5 whenever the heterostructure is formed by two hexagonal lattices. In these cases, the heterointerface can be described using the common surface physics representation. That denotation is dropped when we deal with rectangular lattices, which are better described with the original matrix notation from eq 3. Then, the construction of the supercell is possible just by stacking both sheet crystals following the orientation shown, similar to the specifications in surface physics.[17]

In the majority of combinations, each heterostructure possesses a small strain, which is related to the conversion of its incommensurate matching into a commensurate one by modifying the original lattice parameters by their relative value to obtain approximate solutions of eq 11. In the case of the hexagonal lattices, this value represents the biaxial strain that has to be applied to the primitive basis vectors of both monolayers if this strain is assumed to be distributed equally in magnitude to both layers. This information can be easily retrieved if we have the solution $(\mathbf{m},\mathbf{n})$ from eq 11, which gives us the length of the supercell vectors relative to the original vectors. Therefore, the biaxial strain $\varepsilon = \varepsilon_x = \varepsilon_y$ is obtained when straining both compounds to match the same supercell lattice parameter, i.e., from

$$(1 + \varepsilon)|\mathbf{a}_i||\mathbf{m}| = (1 - \varepsilon)|\mathbf{b}_i||\mathbf{n}|$$

$$\varepsilon = \frac{|\mathbf{b}_i||\mathbf{n}| - |\mathbf{a}_i||\mathbf{m}|}{|\mathbf{b}_i||\mathbf{n}| + |\mathbf{a}_i||\mathbf{m}|} \quad (12)$$

independently of the choice of i, since $|\mathbf{a}_1| = |\mathbf{a}_2|$ and $|\mathbf{b}_1| = |\mathbf{b}_2|$. The application of the strain can be conditioned, when creating the supercell accordingly, to the elastic constants of each separated sheet crystal. In this way, more sensitive materials could be submitted to a smaller strain in order to minimize changes in the band structure of the constituents of the resulting heterostructure.

The results of the coincidence lattice method described above for all the combinations of hexagonal crystals given in Table 1 are summarized in Table S1 of the SI. Despite our limitations to a biaxial strain $\varepsilon < 0.01$ and a unit cell size of the heterostructure with a number of atoms $N \leq 100$ in Table S1 (SI), more than 700 different combinations described by pairs of Wood notations for the two crystals forming the

DOI: 10.1021/acs.jpcc.6b01496
J. Phys. Chem. C 2016, 120, 10895−10908

heterosystems are listed. This variety of bilayers is too large to discuss here. The reader interested in a specific heterocombination will find important details of favorable coincidence lattices in Table S1 (SI). In order to demonstrate the applicability of the general procedure, we focus on the discussion of heterostructures reported experimentally or in other theoretical works. Thereby, the strain in these vdW-bonded heterostructures is only discussed on the basis of the lattice constants given in Table 1. Furthermore, in a few more cases we also discuss supercell sizes with $N > 100$, in order to compare the size of the derived supercells with experimentally observed Moiré patterns, which represent long-range periodicities in the real space. These patterns can easily be treated within the proposed approach. Our predictions for such already studied systems are listed in Table 2. In general, the presented supercells show agreement with those results obtained by other, experimental and theoretical, methods adopted in previous papers concerning structural terms. No total energy calculations, however, have been performed for these bilayer systems. All predictions are based on the coincidence lattice method.

Superior examples for the success of the coincidence lattice method are explored. Indeed, the Moiré pattern predicted for a twisted (θ = 3.3° in Table 2) bilayer of graphene is in agreement with experimental findings.[42] The Moiré pattern and its supercell are represented in Figure 2. The calculated long-range periodicity with 1202 carbon atoms in the supercell gives a lattice constant of 4.27 nm, in good agreement with the measured value of 4.3 nm.[42] In Table 2, a similar agreement is found for graphene on hBN assuming a strain-free situation, despite the fact that the lattice constant of the supercell is much larger, equal to 13.8 nm.[43] Applying the coincidence lattice method with two different strain parameters, we find a perfect agreement with another theoretical work.[43] We also find that a smaller pattern could be formed if a small strain is allowed in both 2D crystals. Other experimental results for the graphene/hBN system can be explained by the coincidence lattice method. Allowing larger cells of coincidence lattices as in Table S1 (SI), our method predicts a Moiré wavelength of 12.4 nm for an interlayer twist of 0.5°, very similar to experimental values around a length of 12.3 nm.[44,45] A reasonable agreement with the size of the formed superlattice can be also noted for the MoS_2/WSe_2 heterobilayer, in which the measurement range is from 4 to 6 times the lattice constants of the monolayers.[46] The calculated lattice constant of 1.45 nm is close to the value derived from the experiment. Coincidences motivated by experimental results are also found for the bilayer MoS_2.[47] The bilayer MoS_2 twisted by 27.8° has a perfect coincidence lattice, due to the equivalence of the lattice parameters, with 78 atoms inside the supercell. The two values are in agreement with the analysis made by Huang and co-workers.[47] The experimental stacking with a twist of 51.5° can be also explained within the coincidence lattice method and calculated lattice parameters, but only with a induced 2.44% strain on each layer.

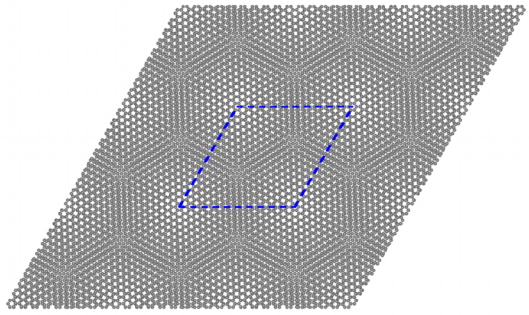

Figure 2. Theoretical Moiré pattern for a twisted bilayer graphene rotated by 3.3° with respect to each other. The lattice parameter of the unit cell, represented by blue dashed lines, is 4.27 nm, in agreement with the experimental result.[42] Carbon atoms are depicted as gray circles, and their spatial distribution leads to bright spots, indicating atoms aligned in the stacking direction, and darker regions, where atoms from one layer fill the empty spots from the other.

In addition to the comparison with measured data, one can also compare supercells applied in total energy calculations. For the bilayer heterostructures studied in refs 6 and 7, we predict different possibilities with varying supercell size, biaxial strain, and twisting angle. Corresponding results are also listed in Table 2. The graphene/MoS_2 heterobilayers from ref 7 demonstrate that the size of the proposed heterostructures is almost the same in terms of relative scaling for each rotation angle. Differences between the two predicted strains can be attributed to lattice optimizations, whose deviations result in varying lattice mismatches. Finally, the ab initio predictions for bilayer heterosystems of MoS_2 with other TMDCs but also graphene and hBN[6] are in agreement with the assortment of supercells derived by our method. However, the coincidence lattice method also finds smaller cells with reasonable strains and fewer atoms inside the resulting supercell, also as a result of variation of the optimized lattice parameters and the assumption of equally distributed strain.

For further illustration of the coincidence lattice method, a selected set of our findings for commensurable heterostructures out of Table S1 (SI) with small strains and supercell sizes is listed in Table 3. All combinations reported in this table are restrained to a distributed strain smaller than 1% and with a maximum number of 30 atoms inside the supercell. For complete information, the reader is still referred to Table S1 (SI).

The coincidence lattices predicted for combinations of two 2D hexagonal crystals in Table 3 illustrate the huge variety of possibilities for investigating heterobilayers made of graphene and transition-metal/group IV dichalcogenides without great computational effort. Intriguing investigations of TMDCs heterobilayers are also feasible with reduced numerical cost. The characteristic twist angles shown in the table, e.g., 0.0°, 30.0°, and 19.1°, are due to the matching of the smaller lengths possible between two lattice points in a hexagonal lattice (e.g., see Figure 1). Most trivial cases, like combinations of the type (1×1)R0°, are excluded in this succinct version of the table. Rotations with redundant angles are also not shown. Since the rotation of a hexagonal lattice by multiples of 60° is symmetry-conserving, we only investigate relative rotations that lie within the interval [0°, 30°], as rotating the hexagonal cell by 30° + φ, $\varphi \in [0°, 30°]$, is equivalent to rotating the cell by −30° + φ.

As stated in the Methodology section, the angle θ denotes the interlayer twist angle between the two investigated lattices. In the case of hexagonal lattices, we define θ = 0° when the primitive vectors from both original lattices are parallel. However, the relation $\theta = \phi_a - \phi_b$ compresses the original information about the two angles in eq 6 to only one. Taking into account general interlayer rotations and point-group operations, one can no longer rely solely on the Wood notation to understand the predicted superstructure as a result

DOI: 10.1021/acs.jpcc.6b01496
J. Phys. Chem. C 2016, 120, 10895−10908

Table 3. Interesting Predictions of Combinations of Hexagonal Crystals Based on the Coincidence Lattice Method[a]

heterobilayer	layer 1	layer 2	θ (deg)	N	ε (%)
Gr/$HfSe_2$	$(\sqrt{7} \times \sqrt{7})$R19.1°	$(\sqrt{3} \times \sqrt{3})$R30.0°	10.9	23	∓0.46
Gr/$MoSe_2$	$(\sqrt{7} \times \sqrt{7})$R19.1°	2 × 2	19.1	26	±0.57
Gr/SnS_2	3 × 3	2 × 2	0.0	30	∓0.45
Gr/$SnSe_2$	$(\sqrt{7} \times \sqrt{7})$R19.1°	$(\sqrt{3} \times \sqrt{3})$R30.0°	10.9	23	±0.82
Gr/WSe_2	$(\sqrt{7} \times \sqrt{7})$R19.1°	2 × 2	19.1	26	±0.49
Gr/ZrS_2	3 × 3	2 × 2	0.0	30	∓0.69
Gr/$ZrSe_2$	$(\sqrt{7} \times \sqrt{7})$R19.1°	$(\sqrt{3} \times \sqrt{3})$R30.0°	10.9	23	∓0.01
hBN/$MoSe_2$	$(\sqrt{7} \times \sqrt{7})$R19.1°	2 × 2	19.1	26	∓0.33
hBN/$HfSe_2$	3 × 3	2 × 2	0.0	30	∓0.45
HfS_2/MoS_2	$(\sqrt{3} \times \sqrt{3})$R30.0°	2 × 2	30.0	21	±0.35
HfS_2/ZrS_2	1 × 1	1 × 1	0.0	6	±0.33
$HfSe_2$/WS_2	$(\sqrt{3} \times \sqrt{3})$R30.0°	2 × 2	30.0	21	∓0.81
$HfSe_2$/WSe_2	$(\sqrt{3} \times \sqrt{3})$R30.0°	2 × 2	30.0	21	±0.95
MoS_2/SnS_2	2 × 2	$(\sqrt{3} \times \sqrt{3})$R30.0°	30.0	21	±0.22
MoS_2/ZrS_2	2 × 2	$(\sqrt{3} \times \sqrt{3})$R30.0°	30.0	21	∓0.02
$MoSe_2$/$SnSe_2$	2 × 2	$(\sqrt{3} \times \sqrt{3})$R30.0°	30.0	21	±0.25
$MoSe_2$/$ZrSe_2$	2 × 2	$(\sqrt{3} \times \sqrt{3})$R30.0°	30.0	21	∓0.58
SnS_2/WS_2	$(\sqrt{3} \times \sqrt{3})$R30.0°	2 × 2	30.0	21	±0.10
$SnSe_2$/WSe_2	$(\sqrt{3} \times \sqrt{3})$R30.0°	2 × 2	30.0	21	∓0.33
WS_2/ZrS_2	2 × 2	$(\sqrt{3} \times \sqrt{3})$R30.0°	30.0	21	∓0.33
WSe_2/$ZrSe_2$	2 × 2	$(\sqrt{3} \times \sqrt{3})$R30.0°	30.0	21	∓0.50

[a]The layer 1 or 2 column relates the original monolayer unit cell to the supercell used in the heterostructure, rotated by an angle θ with respect to each other. The first compound shown in the heterobilayer column is denoted as layer 1. The predicted number N of atoms inside the supercell and the equally distributed biaxial strain ε also characterize the building of the supercell. The ± sign indicates a tensile strain applied on layer 1 and a compressive strain on layer 2, and vice versa for the ∓ sign. Only a set of the supercells containing up to 30 atoms is displayed.

of the rotation of θ applied to the primitive lattice vectors. An example, in which the Wood notation is not specific enough to describe the heterostructure, is the special case in which two identical hexagonal lattices are stacked and one layer is rotated by 27.8° with respect to the other one. To enhance the comprehension of this problem, an enlightening illustration is presented in Figure 3. The problem of comparing two identical

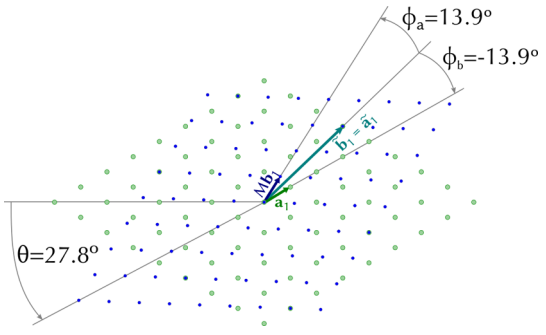

Figure 3. Illustration of two identical hexagonal lattices rotated by 27.8° with respect to each other. Blue and green dots represent each of the Bravais lattices. The angles ϕ_a, ϕ_b, and θ used in the Wood notation are displayed to clarify the notation.

Wood notations for the coincidence lattice of the stacked crystals, in this case, could mislead one to the precipitate conclusion in which $\theta = 0°$, as both layers can be described by the notation $(\sqrt{13} \times \sqrt{13})$R13.9°. Analogous occurrences can also be seen in Tables 2 and S1 (SI). Thus, the angle θ is thoroughly specified in this work to avoid confusion. In Table S1 (SI), redundancy is preferred over the lack of transparency, and equivalent coincidence lattices constructed with different angles θ are also presented.

It is important to note that no information about the stacking order or in-plane translations is given in Tables 1−3 and S1 (SI), as we start from the primitive hexagonal Bravais lattices and do not take the atomic basis of a given 2D crystal into account. Moreover, the stacking order could alter the final geometry under rotations. For instance, for graphene-like materials a AA stacking would become a AB stacking order under a 60° rotation. Also, fractional planar translations of each monolayer system with atoms could alter the stability of the heteroconfiguration. Corresponding space-group operation can be easily done by displacing the atoms inside the original unit cells of the 2D crystals which form the bilayer system. Thus, precise conclusions of system stability require total energy calculations of the complete atomic arrangements, keeping in mind that our listed lattice matchings do not explore directly the possible stackings because only Bravais lattices are studied. This is only possible if the atoms are really taken into consideration, as in explicit total energy calculations.

Until now only combinations of two hexagonal crystals have been investigated. However, the coincidence lattice method presented above can be applied to arbitrary 2D Bravais lattices.[13,16] As an example in which two Bravais lattices with differently shaped primitive cells are used, we inspect the possibility to build coincidence lattices from a rectangular 2D Bravais lattice and a hexagonal one using the approach suggested here. The rectangular lattice was adopted from a 2D phosphorene crystal,[48] whose orthogonal vectors are found to have lengths of 4.504 Å (armchair direction) and 3.305 Å (zigzag direction) within the DFT-optB86b total energy optimization described in the Ab Initio Simulations section.

DOI: 10.1021/acs.jpcc.6b01496
J. Phys. Chem. C 2016, 120, 10895−10908

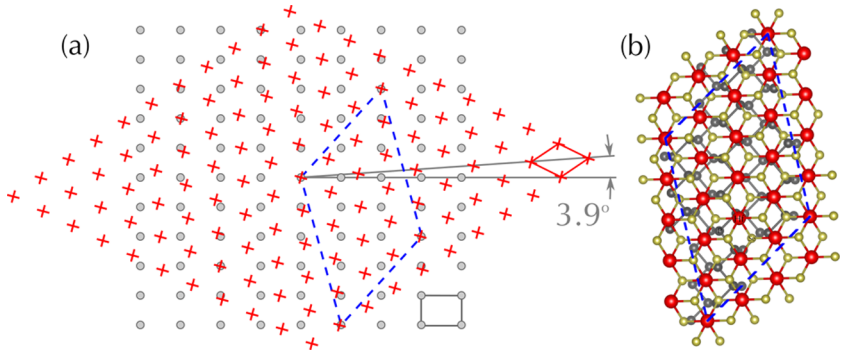

Figure 4. (a) Matching of a $HfSe_2$ hexagonal lattice (red crosses) and a phosphorene rectangular lattice (gray circles) rotated by 3.9° against each other. The original unit cells are drawn with solid lines, and the supercell is denoted by dashed lines. (b) Supercell of the heterostructure with atomic basis. Hafnium, selenium, and phosphorus atoms are displayed in red, yellow, and gray, respectively.

Many combinations with a hexagonal 2D crystal are possible. An illustration of the great action of the coincidence lattice method applied to different Bravais lattices is a heterostructure of $HfSe_2$ on top of phosphorene, whose Bravais and coincidence lattices are shown in Figure 4. In this case, the $HfSe_2$ layer is rotated by 3.9° with respect to the phosphorene armchair orientation and the commensurability is obtained by applying a nonuniform in-plane strain smaller than 1%. In the case of a rectangular/hexagonal combination, however, the resulting strain is not biaxial anymore because the shape of the supercell is different from that of the original ones. Rather, besides different uniaxial strains in the x and y directions, a shear strain appears. One has, therefore, to handle the full 2×2 in-plane deformation tensor $\boldsymbol{\varepsilon}$. Consequently, instead of the simplified Wood notation, the representation of the heterojunction basis asks for the use of the matrix notation, resulting in

$$\mathbf{M}^{a}\begin{bmatrix}\mathbf{a}_1^{\mathrm{T}}\\ \mathbf{a}_2^{\mathrm{T}}\end{bmatrix}=\begin{bmatrix}1 & -5\\ 2 & 3\end{bmatrix}\begin{bmatrix}4.504\ \text{Å} & 0\\ 0 & 3.305\ \text{Å}\end{bmatrix} \tag{13}$$

with $\{\mathbf{a}_1, \mathbf{a}_2\}$ being the primitive vector basis of the phosphorene rectangular lattice. The resulting superlattice is characterized by the matrix $\mathbf{M}^a$ from eq 13.

Applications. For the determination of the actual atomic geometry in a bilayer heterostructure, the presented coincidence lattice method has to be combined with DFT total energy calculations using the constructed supercells listed in Tables 2, 3, and S1 (SI). We demonstrate the applicability of the combined methods to heterobilayer sulfide systems for three examples, also listed in Table 3: (i) a simple, almost lattice-matched heterostructure of HfS_2 and ZrS_2, to illustrate the effect of stacking on the binding energy and interlayer distance; (ii) a heterostructure built from MoS_2 and HfS_2 rotated by 30° against each other; and (iii) a similar heterostructure made by MoS_2 and ZrS_2 rotated by 30° against each other.

The simplest case investigated is the almost lattice-matched HfS_2 and ZrS_2 heterobilayer system. In order to test the influence of strain on isolated layers, we studied the maximum 0.66% biaxial strain on HfS_2. However, no significant changes have been observed in the electronic properties of this material, as expected from previous studies.[33] Therefore, only weak strain-induced modifications are expected for the behavior of the bilayer system. We investigated four different stackings possible for the HfS_2/ZrS_2 bilayer arrangement with 1T-structure layers, T, C7, C27, and AA,[49] thereby keeping the original 1×1 translational symmetry (refer to Table 3). The influence of the stacking on interlayer separation, in-plane translations, and binding energy is of interest. The stacking geometries (top and side views) are depicted in Figure 5a. The energetics of the bilayer system versus the interlayer distance and the relative lateral displacement of the two 2D crystals are illustrated in parts b and c of Figure 5, respectively.

The plot of binding energy versus distance between HfS_2 and ZrS_2 in Figure 5b shows that the stackings AA, C7, and T are more stable than the C27 configuration. This results in a smaller interlayer distance of about 3.0 Å compared to the 3.5 Å in the C27 case. However, despite the fixed coincidence lattice, also the relative lateral atomic arrangements influence the stability of the bilayer systems. Small in-plane displacements executed, keeping constant the interlayer distance of AA and C7 stackings of the two 2D crystals 1T-HfS_2 and 1T-ZrS_2, demonstrate in Figure 5c the local stability of these arrangements, contrary to the C27 one. The total energy curves do not exhibit pronounced minima, and the stackings are not very rigid. The T stacking can be turned into an AA stacking with a significant displacement in the $[\bar{1}100]$ direction, which also lowers the equilibrium interlayer distance (compare the two structures in Figure 5a) and explains the absence of a local energy minimum for this stacking. Total force calculations indicate that repulsion between close sulfur atoms makes the C27 configuration unstable against in-plane shifts in the $[\bar{1}100]$ direction. The calculated binding energies lie between 15.6 and 22.2 meV/Å^2, values which are very reasonable energies for vdW-bonded TMDCs bilayers.[50] The stability of even the least energetically favorable stacking, therefore, is in agreement with the success of the preparation of such vdW-bonded heterostructures in several experiments. The weak vdW bonding and the formation of coincidence lattices allow the easy preparation of stacked heterostructures from exfoliated 2D materials, despite the mismatch in the lattice constants, bonding, and even crystal structure.

The influence of the actual stacking and atomic geometry of the heterostructure on the electronic structure has been studied by means of the band structure and the alignment of the electronic states of the two isolated 2D crystals in the heterocombination. For illustration of this geometric influence, the corresponding band structures are calculated for the four stackings of HfS_2/ZrS_2. As an example, the band structure of the AA stacking is displayed in Figure 6a. Using a projection technique, the band structures of HfS_2 and ZrS_2 in the

DOI: 10.1021/acs.jpcc.6b01496
J. Phys. Chem. C 2016, 120, 10895−10908

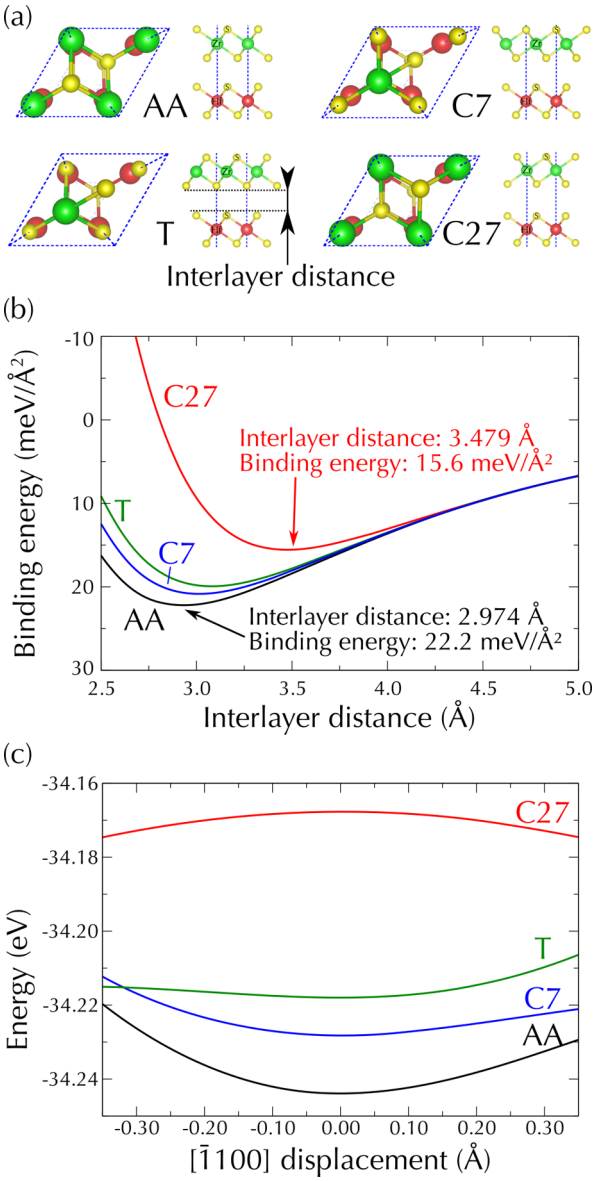

Figure 5. (a) Four different stackings investigated for the HfS_2 and ZrS_2 heterostructure. Zirconium, hafnium, and sulfur are depicted in green, red, and yellow, respectively, and the dashed lines detail the supercell edges. (b) Total energy of the supercell for the different stackings, showing a stable configuration for each one of them. (c) Total energy of the supercells on their own equilibrium interlayer distance for small displacements in the $[\bar{1}100]$ direction.

heterostructure are extracted and presented in different colors. This technique allows us to derive the local energy gap (E_g), the valence band maximum (VBM or $-I$) at Γ, and the conduction band minimum (CBM or $-A$) at M in the BZ of the two materials for each given stacking, strain and, hence, the vdW interactions. The corresponding results are summarized in Table 4. The stacking and bilayer influences follow from a comparison with the corresponding quantities of the free-standing 2D crystals in Table 1. Indeed, the values E_g, A, and I are influenced by the heterocombination. We have to point out that a similar influence due to stacking in Table 4 has been recently observed experimentally for the interlayer twist in the graphene/MoS_2 system.[51] The differences in the CBM and VBM values in Table 4 define the true band discontinuities between materials 1 and 2

$$\Delta E_v = \mathrm{VBM}(2) - \mathrm{VBM}(1)$$
$$\Delta E_c = \mathrm{CBM}(1) - \mathrm{CBM}(2) \quad (14)$$

in the heterostructure. They can be compared with the natural band discontinuities

$$\Delta E_v^{\mathrm{nat}} = I(1) - I(2)$$
$$\Delta E_c^{\mathrm{nat}} = A(2) - A(1) \quad (15)$$

by applying the vacuum level alignment[17,52] and the characteristic energies from Table 1. The band discontinuities characterize a type I (II) heterostructure as $\Delta E_v \Delta E_c > 0$ ($\Delta E_v \Delta E_c < 0$).

The energy differences in the band gaps and positions of band extrema (see Table 4) and, hence, band discontinuities are inferior to 0.10 eV between different stackings, suggesting only a little charge transfer through the interface between the two sheet crystals HfS_2 and ZrS_2. However, this trend is not monotonous. This observation is supported by the almost unchanging electronic properties of the two materials when comparing the values in Tables 1 and 4. Thereby, the influence of the most stable AA, C7, and T stackings and the details of the atomic geometry on the VBM positions is negligibly small. The main effect of the heterostructure is the absolute shifts of the VBM of HfS_2 (ZrS_2) of about 0.08 (0.02) eV toward lower (higher) energies with respect to the freestanding situations. The opposite behavior is found for the CBM. As a consequence, the gap of HfS_2 (ZrS_2) is opened (shrunk) compared to the isolated situation along the row AA, C7, and T. These small shifts, however, have important consequences for the predicted heterostructure behavior. In comparison to the type II expectation for the pristine monolayers with the natural band discontinuities $\Delta E_v^{\mathrm{nat}} = -33$ meV and $\Delta E_c^{\mathrm{nat}} = 213$ meV from Table 1, the real junctions change from type II to type I due to vdW interactions and the small valence band offset already visible from the natural band alignment. For instance, in the AA case, band discontinuities $\Delta E_v = 79$ meV and $\Delta E_c = 193$ meV occur. This fact is accompanied by an increase in the band gap of HfS_2 and a decrease in the band gap of ZrS_2 in the heterostructure.

For the purpose of better understanding the influence of interlayer interactions in band alignments, we have inspected the formation of the bands from the original HfS_2 and ZrS_2 monolayers. Considering the similarities shared by these two TMDCs and perceiving that their bands are generated within the same crystal structure, we depict the nature of the bands and their orbital character only for HfS_2 in Figure 6b. The formation of the bands for ZrS_2 is analogous and hence not explicitly shown. It is possible to explain the almost invariant band gap and band discontinuities in the heterobilayer by recognizing the predominance of localized cation d orbitals in the CBM and in-plane anion $p_x + p_y$ states in the VBM, which overlap less with the states from the other layer, in contrast to the p_z orbitals. In fact, the greatest alterations are seen near the BZ boundary, in which the predominance of p_z orbitals in the valence band affects more the electronic properties of the vdW-bonded heterostructure and hence interlayer separation and stacking order. Stackings in which p_z orbitals prevail in the band formation, such as phosphorene or graphene, suffer pronounced changes in the electronic structure due to these interlayer interactions.[53] We also observe a mixture of orbitals at the conduction band minimum near the M point, made

DOI: 10.1021/acs.jpcc.6b01496
J. Phys. Chem. C 2016, 120, 10895−10908

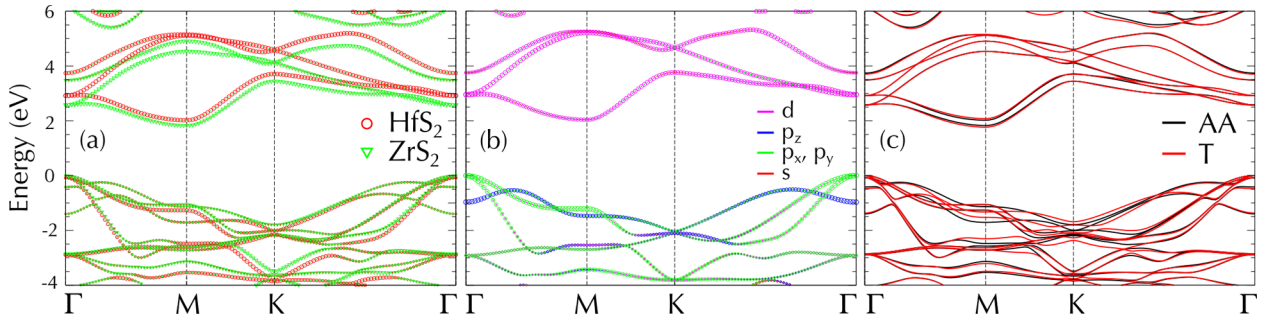

Figure 6. (a) Band structure of HfS_2/ZrS_2 heterostructure with AA stacking projected onto each layer. Contributions from HfS_2 are shown with red circles and those from ZrS_2 are displayed with green triangles. The size of the marker indicates the relative contribution from each monolayer to the total band structure. (b) Orbital character of the band states of pristine HfS_2. (c) Influence of different HfS_2/ZrS_2 stackings on the heterobilayer band structures.

Table 4. Characteristic Electronic Energies of HfS_2 and ZrS_2 in a vdW-Bonded Heterostructure with Interface[a]

	HfS_2			ZrS_2		
stacking	CBM (eV)	VBM (eV)	E_g (eV)	CBM (eV)	VBM (eV)	E_g (eV)
monolayer	−4.925	−6.956	2.03	−5.138	−6.989	1.85
AA	−4.951	−7.049	2.10	−5.144	−6.970	1.83
C7	−4.944	−7.040	2.10	−5.157	−6.971	1.81
T	−4.887	−7.035	2.15	−5.201	−6.965	1.76
C27	−4.785	−6.922	2.14	−5.064	−6.859	1.80

[a]The projection technique illustrated in Figure 6a is used to extract values for the individual 2D crystals. The conduction band minimum (CBM) and valence band maximum (VBM) are taken with respect to the vacuum level. The band gap (E_g) is the energy difference between the CBM and VBM for each monolayer in the heterojunction. The energies from isolated monolayers are also shown for ease of comparison.

predominantly from d_{z^2} and d_{yz} orbitals of the cations. As the stacking goes from the most stable configuration to the least stable one, i.e., from AA to C27, we increase the repulsion between these orbitals from each layer, thus slightly modifying the fundamental band gap of each 2D crystal. The T stacking, however, leads to the larger shifts in the band gaps due the smaller distance between each layers' cations (Hf or Zr) and the sulfur anions. These shifts are more directly shown in Table 4 and depicted in Figure 6c.

Despite the weak vdW interactions between the two layered crystals not significantly changing the band gaps of each layer constituting the heterointerface, transitions between heterostructure types may happen through their direct contact if the natural band line-ups are characterized by only small band offsets. Interaction-induced changes in the valence or conduction band created by interlayer interactions and orbital overlaps can surmount these natural band alignments and force the transition between a type II to a type I heterostructure or vice versa, depending on the sensitivity of each layer to orbitals overlapping and charge transfer. Modulation of these properties via external factors, however, such as piezoelectricity,[54] electric field,[55] or interface decoupling[46] may also be employed to fine-tune the interface properties.

The same kind of total energy optimizations, electronic band structure calculations, and electronic structure investigations have also been applied to the vdW-bonded HfS_2 or $ZrS_2(\sqrt{3} \times \sqrt{3})R30°$ on $MoS_2(2 \times 2)$ heterosystem (see Table 3). As a supercell in real space, i.e., a nonprimitive unit cell of the original crystal lattice, is used, the resulting reciprocal space vectors shrink with respect to the original ones. This leads to band structures folded onto the small Brillouin zone of the coincidence lattice, but without changes in the fundamental electronic properties of each isolated monolayer. The coincidence lattice and the atomic geometry resulting in the HfS_2/MoS_2 case are presented in Figure 7. The two heterocombinations are not lattice-constant-matched and, therefore, are good examples for application of the coincidence lattice method to construct supercells in the first step. In the subsequent total energy calculations of the atomic geometries, we have assumed that the entire strain appears in the MoS_2 2D crystal. Only a few electronic changes are observed, e.g., the band gap of MoS_2 changing from 2.25 to 2.31 eV while its direct gap character is kept at K. This increase in the MoS_2 gap is due the small compressive strain and has also been predicted in previous studies.[33] The vdW coupling of the two layers lowers the total energy of the supercell, and a stable

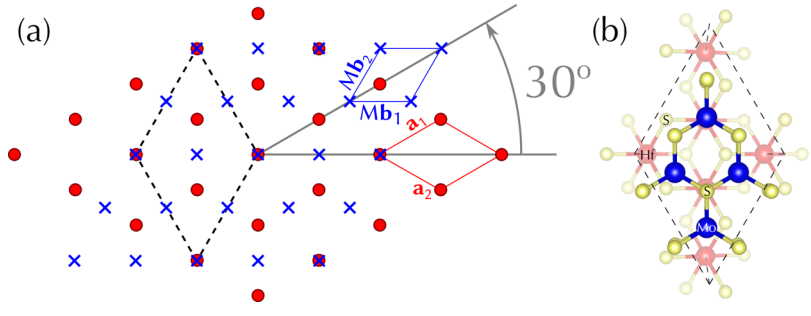

Figure 7. (a) Matching of a MoS_2 lattice (blue crosses) and a HfS_2 lattice (red circles) under a relative rotation of 30° and (b) the supercell generated in this case. Molybdenum, hafnium, and sulfur atoms are depicted in blue, red, and yellow, respectively.

DOI: 10.1021/acs.jpcc.6b01496
J. Phys. Chem. C 2016, 120, 10895−10908

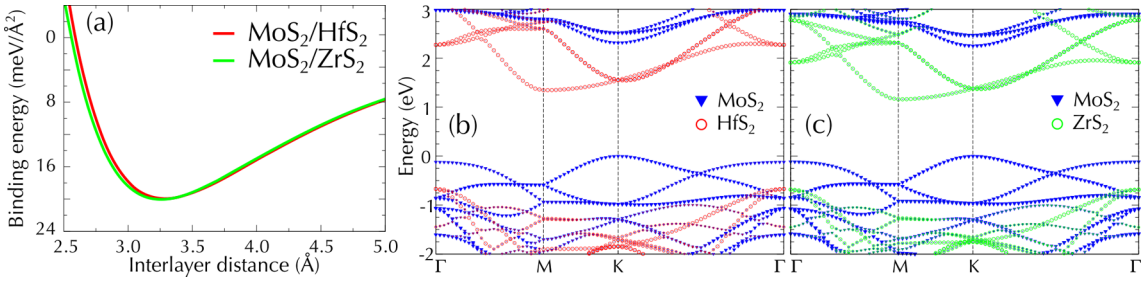

Figure 8. (a) Binding energy of the MoS_2 on top of HfS_2 and ZrS_2 per unit area versus the interlayer distance. For each equilibrium position, band structures projected onto each monolayer are given for the (b) MoS_2 and HfS_2 and (c) MoS_2 and ZrS_2 heterostructure calculated for the lowest-energy arrangements. Relative sizes of markers indicate the percentual composition of each band from each material.

configuration is found with an interlayer distance of 3.329 Å for the HfS_2/MoS_2 system and 3.299 Å for the ZrS_2/MoS_2 system, respectively, with a binding energy of 20 meV/Å^2 in both cases, as shown in Figure 8a. The total energy of the layer stacking does not change by values larger than 1 meV when lateral atomic displacements are made in any lateral direction. Thus, the heterostructures are independent of any relative translation of the two atomic layers against each other, as long as the coincidence lattice remains fixed. Comparing with the larger energy variations predicted for other MoS_2-including hetero-systems,[50] we conclude that the two studied heterobilayers are stable with a given coincidence lattice but rather invariant against planar translations. The two systems are examples in which the lattice mismatch creates a spatially distributed stacking arrangement, leading to an energy gain due to the interface binding, regardless of their relative lateral positions.

The electronic properties of the two heterostructures are displayed in Figure 8b,c. We observe the direct character of the MoS_2 band gap, while the indirect band gap of the HfS_2 (ZrS_2) suffers a reduction of 0.1 eV. We find a valence band offset of ΔE_v = 0.67 eV (0.68 eV) and a conduction band offset of ΔE_c = −0.97 eV (−1.09 eV) for the HfS_2/MoS_2 (ZrS_2/MoS_2) system. The comparison with the natural band discontinuities ΔE_v^{nat} = 0.65 eV/ΔE_c^{nat} = −0.86 eV (MoS_2/HfS_2) and ΔE_v^{nat} = 0.69 eV/ΔE_c^{nat} = −1.07 eV (MoS_2/ZrS_2) from Table 1 shows that the two heterostructures preserve the natural band alignments of the individual materials given in Table 1, i.e., a type II heterocharacter, despite the relative rotation imposed on the simulated supercell and the vdW bonding. The small difference between the natural band discontinuities and the values obtained from the simulated interface in the HfS_2/MoS_2 heterojunction is due the small strain induced in MoS_2 needed to compose a commensurate system.

The projected band structures for both simulated hetero-interfaces in Figure 8b,c not only show the character of the band gaps in the *k*-space for the "isolated" 2D crystals but also clearly indicate the indirect character of the band gaps of the heterostructure in real space. While the CBM appears at M in the HfS_2 or ZrS_2 layer, the VBM at K is defined by the MoS_2 system. The projection technique illustrates the low influence of vdW interactions on the electronic structures of these heterostructures by the very localized band states, which do not indicate reasonable state mixing or electron transfers. The latter phenomena occurs only at symmetry points where the band states are constituted mainly by p_z orbitals, as in the case of the heterostructure band originated from the valence band states of HfS_2 or ZrS_2. This band is composed with significant contributions from both layers and undergo a transition between the M and K points. In the band structures from Figure 8b,c, this is evidenced by the shrinkage of the circles, i.e. the percentage of orbitals from the HfS_2 or ZrS_2 layer, and the increase of the size of blue triangles. Conductions band, whose character is based predominantly on d orbitals, do not withstand appreciable changes.

IV. SUMMARY AND CONCLUSIONS

In summary, we have presented a general method for finding small supercells of heterostructures made from 2D materials for studying their properties. On the basis of the idea of the existence of a coincidence lattice in the context of 2D Bravais lattices, we have calculated vdW-bonded heterostructures among TMDCs, group IV dichalcogenides, graphene, and hBN using the results of the coincidence lattice method and taking the atoms into account. The method starts from nonprimitive unit cells of each sheet crystal in the heterocombination, which correspond to superlattice geometries due to the reconstruction in surface physics and can therefore be described by either the matrix or Wood notation. Within the coincidence lattice method a system of diophantine equations has to be solved to find optimized lattice geometries of bilayers. The optimization criterion is to find small joint supercells with only an almost vanishing in-plane strain in the two 2D crystals. We validated this approach by comparing its results with those of already studied systems by showing its compatibility with simpler procedures. As an interesting fact, Moiré patterns found experimentally for van der Waals-bonded bilayer systems could be explained by coincidence lattices. We found a large set of interesting coincidence lattices and corresponding supercells using rotations and strain to transform the original combination into a commensurate one. We demonstrated how the small supercells can be applied to simulate real heterojunctions of two sheet crystals. As examples for application of results of the coincidence lattice method, we investigated three heterostructures made from the TMDCs HfS_2, ZrS_2, and MoS_2 using the predicted small supercells, within ab initio total energy and electronic structure methods in more detail. For the three explored combinations, we showed that the heterostructures are indeed stabilized by vdW interaction. The coincidence lattices filled with the atoms really lead to flat local minima on the total energy surface. The resulting stacking and repulsive effects lead to small influences on the final electronic structure. More importantly, the individual electronic properties are almost preserved upon contact of the two constituent materials, which certify the promising characteristics from van der Waals heterostructures. Nevertheless, the small interactions between the two 2D crystals in the heterostructure may change the heterostructure from type II to type I.

DOI: 10.1021/acs.jpcc.6b01496
J. Phys. Chem. C 2016, 120, 10895−10908

■ ASSOCIATED CONTENT

Supporting Information

The Supporting Information is available free of charge on the ACS Publications website at DOI: 10.1021/acs.jpcc.6b01496.

Full table containing predictions of coincidence lattices based on TMDCs, group IV dichalcogenides, graphene, and group III−V compounds studied in this work (PDF)

■ AUTHOR INFORMATION

Corresponding Authors

*D.S.K.: e-mail, danielskoda@gmail.com.
*F.B.: e-mail, friedhelm.bechstedt@uni-jena.de.
*M.M.: e-mail, mmarques@ita.br.
*L.K.T.: e-mail, lkteles@ita.br; phone, +55 12 3947-5849.

Notes

The authors declare no competing financial interest.

■ ACKNOWLEDGMENTS

We kindly thank J. Furthmüller, R. R. Pelá, and L. Matthes for the discussions and advice. This work was supported by the Brazilian funding agencies CNPq (scholarship grant) and CAPES (PVE Grant No. 88881.068355/2014-01 and scholarship grant) within the program Science Without Borders.

■ REFERENCES

(1) Butler, S. Z.; Hollen, S. M.; Cao, L.; Cui, Y.; Gupta, J. A.; Gutiérrez, H. R.; Heinz, T. F.; Hong, S. S.; Huang, J.; Ismach, A. F.; et al. Progress, Challenges, and Opportunities in Two-Dimensional Materials Beyond Graphene. *ACS Nano* **2013**, *7*, 2898−2926.

(2) Wang, Q. H.; Kalantar-Zadeh, K.; Kis, A.; Coleman, J. N.; Strano, M. S. Electronics and optoelectronics of two-dimensional transition metal dichalcogenides. *Nat. Nanotechnol.* **2012**, *7*, 699−712.

(3) Xu, M.; Liang, T.; Shi, M.; Chen, H. Graphene-like two-dimensional materials. *Chem. Rev.* **2013**, *113*, 3766−3798.

(4) Geim, A.; Grigorieva, I. Van der Waals heterostructures. *Nature* **2013**, *499*, 419−425.

(5) Yu, P.; Cardona, M. *Fundamentals of Semiconductors: Physics and Materials Properties*; Graduate Texts in Physics; Springer-Verlag: Berlin, 2010.

(6) Komsa, H.-P.; Krasheninnikov, A. V. Electronic structures and optical properties of realistic transition metal dichalcogenide heterostructures from first principles. *Phys. Rev. B: Condens. Matter Mater. Phys.* **2013**, *88*, 085318.

(7) Wang, Z.; Chen, Q.; Wang, J. Electronic Structure of Twisted Bilayers of Graphene/MoS2 and MoS2/MoS2. *J. Phys. Chem. C* **2015**, *119*, 4752−4758.

(8) van der Zande, A. M.; Kunstmann, J.; Chernikov, A.; Chenet, D. A.; You, Y.; Zhang, X.; Huang, P. Y.; Berkelbach, T. C.; Wang, L.; Zhang, F.; et al. Tailoring the Electronic Structure in Bilayer Molybdenum Disulfide via Interlayer Twist. *Nano Lett.* **2014**, *14*, 3869−3875.

(9) Shi, Y.; Zhou, W.; Lu, A.-Y.; Fang, W.; Lee, Y.-H.; Hsu, A. L.; Kim, S. M.; Kim, K. K.; Yang, H. Y.; Li, L.-J.; et al. van der Waals Epitaxy of MoS2 Layers Using Graphene As Growth Templates. *Nano Lett.* **2012**, *12*, 2784−2791.

(10) Woods, C. R.; Britnell, L.; Eckmann, A.; Ma, R. S.; Lu, J. C.; Guo, H. M.; Lin, X.; Yu, G. L.; Cao, Y.; Gorbachev, R. V.; et al. Commensurate-incommensurate transition in graphene on hexagonal boron nitride. *Nat. Phys.* **2014**, *10*, 451−456.

(11) Kolmogorov, A. N.; Crespi, V. H. Registry-dependent interlayer potential for graphitic systems. *Phys. Rev. B: Condens. Matter Mater. Phys.* **2005**, *71*, 235415.

(12) Kohn, W.; Sham, L. J. Self-consistent equations including exchange and correlation effects. *Phys. Rev.* **1965**, *140*, A1133−A1138.

(13) Bechstedt, F.; Enderlein, R. *Semiconductor Surfaces and Interfaces: Their Atomic and Electronic Structures (Physical Research)*; Akademie-Verlag: Berlin, 1988.

(14) Lazić, P. CellMatch: Combining two unit cells into a common supercell with minimal strain. *Comput. Phys. Commun.* **2015**, *197*, 324−334.

(15) Weckbecker, D.; Shallcross, S.; Fleischmann, M.; Ray, N.; Sharma, S.; Pankratov, O. Low-energy theory for the graphene twist bilayer. *Phys. Rev. B: Condens. Matter Mater. Phys.* **2016**, *93*, 035452.

(16) Kittel, C. *Introduction to Solid State Physics*; Wiley: New York, 2004.

(17) Bechstedt, F. *Principles of Surface Physics*; Springer-Verlag: Berlin, 2003.

(18) Wood, E. A. Vocabulary of surface crystallography. *J. Appl. Phys.* **1964**, *35*, 1306−1312.

(19) Kresse, G.; Furthmüller, J. Efficiency of ab-initio total energy calculations for metals and semiconductors using a plane-wave basis set. *Comput. Mater. Sci.* **1996**, *6*, 15−50.

(20) Kresse, G.; Furthmüller, J. Efficient iterative schemes for ab initio total-energy calculations using a plane-wave basis set. *Phys. Rev. B: Condens. Matter Mater. Phys.* **1996**, *54*, 11169−11186.

(21) Blöchl, P. E. Projector augmented-wave method. *Phys. Rev. B: Condens. Matter Mater. Phys.* **1994**, *50*, 17953−17979.

(22) Kresse, G.; Joubert, D. From ultrasoft pseudopotentials to the projector augmented-wave method. *Phys. Rev. B: Condens. Matter Mater. Phys.* **1999**, *59*, 1758−1775.

(23) Perdew, J. P.; Burke, K.; Ernzerhof, M. Generalized gradient approximation made simple. *Phys. Rev. Lett.* **1996**, *77*, 3865−3868.

(24) Klimeš, J.; Bowler, D. R.; Michaelides, A. Van der Waals density functionals applied to solids. *Phys. Rev. B: Condens. Matter Mater. Phys.* **2011**, *83*, 195131.

(25) Björkman, T. Testing several recent van der Waals density functionals for layered structures. *J. Chem. Phys.* **2014**, *141*, 074708.

(26) Monkhorst, H. J.; Pack, J. D. Special points for Brillouin-zone integrations. *Phys. Rev. B* **1976**, *13*, 5188−5192.

(27) Paier, J.; Marsman, M.; Hummer, K.; Kresse, G.; Gerber, I. C.; Ángyán, J. G. Screened hybrid density functionals applied to solids. *J. Chem. Phys.* **2006**, *124*, 154709.

(28) Paier, J.; Marsman, M.; Hummer, K.; Kresse, G.; Gerber, I.; Ángyán, J. Erratum: "Screened hybrid density functionals applied to solids" [J. Chem. Phys. 124, 154709 (2006)]. *J. Chem. Phys.* **2006**, *125*, 249901.

(29) Heyd, J.; Scuseria, G. E.; Ernzerhof, M. Hybrid functionals based on a screened Coulomb potential. *J. Chem. Phys.* **2003**, *118*, 8207−8215.

(30) Heyd, J.; Scuseria, G. E.; Ernzerhof, M. Erratum: "Hybrid functionals based on a screened Coulomb potential" [J. Chem. Phys. 118, 8207 (2003)]. *J. Chem. Phys.* **2006**, *124*, 219906.

(31) Bechstedt, F. *Many-Body Approach to Electronic Excitations*; Springer-Verlag: Berlin, 2015.

(32) Momma, K.; Izumi, F. *VESTA*: A three-dimensional visualization system for electronic and structural analysis. *J. Appl. Crystallogr.* **2008**, *41*, 653−658.

(33) Guzman, D. M.; Strachan, A. Role of strain on electronic and mechanical response of semiconducting transition-metal dichalcogenide monolayers: An ab-initio study. *J. Appl. Phys.* **2014**, *115*, 243701.

(34) Zhuang, H. L.; Hennig, R. G. Computational search for single-layer transition-metal dichalcogenide photocatalysts. *J. Phys. Chem. C* **2013**, *117*, 20440−20445.

(35) Lin, Y.-C.; Dumcenco, D. O.; Huang, Y.-S.; Suenaga, K. Atomic mechanism of the semiconducting-to-metallic phase transition in single-layered MoS2. *Nat. Nanotechnol.* **2014**, *9*, 391−396.

(36) Wen, S.; Pan, H.; Zheng, Y. Electronic properties of tin dichalcogenide monolayers and effects of hydrogenation and tension. *J. Mater. Chem. C* **2015**, *3*, 3714−3721.

(37) Luo, H.; Xie, W.; Tao, J.; Inoue, H.; Gyenis, A.; Krizan, J. W.; Yazdani, A.; Zhu, Y.; Cava, R. J. Polytypism, polymorphism, and superconductivity in TaSe2- xTex. *Proc. Natl. Acad. Sci. U. S. A.* **2015**, *112*, E1174−E1180.

DOI: 10.1021/acs.jpcc.6b01496
J. Phys. Chem. C 2016, 120, 10895−10908

(38) Lee, C.-H.; Silva, E. C.; Calderin, L.; Nguyen, M. A. T.; Hollander, M. J.; Bersch, B.; Mallouk, T. E.; Robinson, J. A. Tungsten Ditelluride: a layered semimetal. *Sci. Rep.* **2015**, *5*, 10013.
(39) Qiu, D. Y.; da Jornada, F. H.; Louie, S. G. Optical spectrum of MoS2: many-body effects and diversity of exciton states. *Phys. Rev. Lett.* **2013**, *111*, 216805.
(40) Gronvold, F.; Haraldsen, H.; Kjekshus, A. On the sulfides, selenides and tellurides of platinum. *Acta Chem. Scand.* **1960**, *14*, 1879−1893.
(41) Madelung, O., Rössler, U., Schulz, M., Eds. *Non-Tetrahedrally Bonded Elements and Binary Compounds I*; Landolt−Börnstein—Group III Condensed Matter; Springer: Berlin, 1998; Vol. *41C*, pp 1−3.
(42) Brihuega, I.; Mallet, P.; González-Herrero, H.; Trambly de Laissardière, G. T.; Ugeda, M.; Magaud, L.; Gómez-Rodríguez, J.; Ynduráin, F.; Veuillen, J.-Y. Unraveling the intrinsic and robust nature of van Hove singularities in twisted bilayer graphene by scanning tunneling microscopy and theoretical analysis. *Phys. Rev. Lett.* **2012**, *109*, 196802.
(43) Slotman, G.; van Wijk, M.; Zhao, P.-L.; Fasolino, A.; Katsnelson, M.; Yuan, S. Effect of structural relaxation on the electronic structure of graphene on hexagonal boron nitride. *Phys. Rev. Lett.* **2015**, *115*, 186801.
(44) Tang, S.; Wang, H.; Zhang, Y.; Li, A.; Xie, H.; Liu, X.; Liu, L.; Li, T.; Huang, F.; Xie, X.; et al. Precisely aligned graphene grown on hexagonal boron nitride by catalyst free chemical vapor deposition. *Sci. Rep.* **2013**, *3*, 2666.
(45) Wang, D.; Chen, G.; Li, C.; Cheng, M.; Yang, W.; Wu, S.; Xie, G.; Zhang, J.; Zhao, J.; Lu, X.; et al. Thermally Induced Graphene Rotation on Hexagonal Boron Nitride. *Phys. Rev. Lett.* **2016**, *116*, 126101.
(46) Fang, H.; Battaglia, C.; Carraro, C.; Nemsak, S.; Ozdol, B.; Kang, J. S.; Bechtel, H. A.; Desai, S. B.; Kronast, F.; Unal, A. A.; et al. Strong interlayer coupling in van der Waals heterostructures built from single-layer chalcogenides. *Proc. Natl. Acad. Sci. U. S. A.* **2014**, *111*, 6198−6202.
(47) Huang, S.; Ling, X.; Liang, L.; Kong, J.; Terrones, H.; Meunier, V.; Dresselhaus, M. S. Probing the interlayer coupling of twisted bilayer MoS2 using photoluminescence spectroscopy. *Nano Lett.* **2014**, *14*, 5500−5508.
(48) Liu, H.; Neal, A. T.; Zhu, Z.; Luo, Z.; Xu, X.; Tománek, D.; Ye, P. D. Phosphorene: an unexplored 2D semiconductor with a high hole mobility. *ACS Nano* **2014**, *8*, 4033−4041.
(49) Kośmider, K.; Fernández-Rossier, J. Electronic properties of the MoS2-WS2 heterojunction. *Phys. Rev. B: Condens. Matter Mater. Phys.* **2013**, *87*, 075451.
(50) Björkman, T.; Gulans, A.; Krasheninnikov, A. V.; Nieminen, R. M. van der Waals bonding in layered compounds from advanced density-functional first-principles calculations. *Phys. Rev. Lett.* **2012**, *108*, 235502.
(51) Jin, W.; Yeh, P.-C.; Zaki, N.; Chenet, D.; Arefe, G.; Hao, Y.; Sala, A.; Mentes, T. O.; Dadap, J. I.; Locatelli, A.; et al. Tuning the electronic structure of monolayer graphene/MoS2 van der Waals heterostructures via interlayer twist. *Phys. Rev. B: Condens. Matter Mater. Phys.* **2015**, *92*, No. 201409(R).
(52) Mönch, W. *Electronic Properties of Semiconductor Interfaces*; Springer-Verlag: Berlin, 2004.
(53) Padilha, J.; Fazzio, A.; da Silva, A. J. Van der Waals heterostructure of phosphorene and graphene: Tuning the Schottky barrier and doping by electrostatic gating. *Phys. Rev. Lett.* **2015**, *114*, 066803.
(54) Huang, L.; Li, Y.; Wei, Z.; Li, J. Strain induced piezoelectric effect in black phosphorus and MoS2 van der Waals heterostructure. *Sci. Rep.* **2015**, *5*, 16448.
(55) Huang, L.; Huo, N.; Li, Y.; Chen, H.; Yang, J.; Wei, Z.; Li, J.; Li, S.-S. Electric-Field Tunable Band Offsets in Black Phosphorus and MoS2 van der Waals p-n Heterostructure. *J. Phys. Chem. Lett.* **2015**, *6*, 2483−2488.

DOI: 10.1021/acs.jpcc.6b01496
J. Phys. Chem. C 2016, 120, 10895−10908